

Cluster-Based Nonuniform Transformation Field Analysis of Graphene Nanocomposites

Yinan JIANG*, Juanjuan CHEN**, Lihua LIANG*, Yangjian XU*, Xiaozhe JU*

*College of Mechanical Engineering, Zhejiang University of Technology, Hangzhou 310023, China,

E-mail: xju@zjut.edu.cn (Corresponding author)

**Zhejiang Huayun Information Technology Co., Ltd., Hangzhou 310000, China

<https://doi.org/10.5755/j02.mech.33191>

1. Introduction

Composite materials are a kind of materials composed of two or more materials with different chemical and physical properties. It is widely used in industry, and has high strength, high modulus and high fatigue resistance [1]. Graphene, due to its superior properties such as large specific surface area, excellent mechanical properties, good conductivity and heat conduction as well as excellent flame retardancy etc., has become a very popular reinforcement material in recent years, widely used in aerospace, automobile and shipbuilding industries [2–4]. Adding graphene to the resin matrix can greatly improve the strength, and research on the properties of graphene nanocomposites is still a recent topic.

In structural analysis, materials are often regarded as homogeneous. However, on the microscale, this homogeneity is lost. This microheterogeneity affects the macroscopic performance to a large extent. In order to deeply understand the mechanical properties of composite materials and save experimental costs, the multiscale calculation method towards macro-microscale coupling is very effective [5,6]. In microscale analysis, the most direct method to predict the mechanical behavior of nonlinear heterogeneous materials is numerical method, such as finite element method (FEM) [7], which is applicable to complex micro structures and arbitrary complex constitutive relations [8, 9]. However, for large structural analysis, the huge amount of computational costs and storage requirements makes this method infeasible. In order to improve the computational efficiency, Dvorak et al. [10] proposed the so-called Transform Field Analysis (TFA) method, which treats the inelastic strain field approximately as a piecewise uniform field. However, in some cases, the accuracy is insufficient [11]. For this reason, Michel and Suquet [12] proposed the nonuniform transformation field analysis (NTFA) method, taking into account the nonuniform distribution of microscopic field quantities [13]. Later, Ju et al. extended the NTFA to describe softening effects and strength differences in [14, 15]. Liu et al. [16, 17] proposed self-consistent cluster analysis (SCCA) to overcome some shortcomings of the NTFA. The method consists of two steps: firstly, the spatial domain is divided according to the clustering analysis of linear elastic strain localization operators; then, an analysis process similarly to the TFA is applied to the subdomain. The recent works of [18, 19] combined reduced order models including the NTFA with clustering algorithm and proposed a new cluster-based reduced order model.

The purpose of this paper is to integrate a clustering analysis into the NTFA method to solve the problems of low universality and high application threshold of this method, and then propose a new reduced order model, which will be used to predict the macroscopic properties of graphene nanocomposites. The paper is organized as follows. Firstly, the NTFA method is introduced briefly. Cluster-based nonuniform transformation analysis (CNTFA) in [19] is then introduced, while the derivation and numerical implementation are revealed in detail. Finally, the method will be investigated by several numerical experiments, where the mechanical properties of graphene nanocomposites are studied.

2. Basic formulation of the two scale problem

On the premise that the macroscopic characteristic length L is much larger than the microscopic one l , based on the scale separation assumption [20], a two-scale problem is shown in Fig. 1.

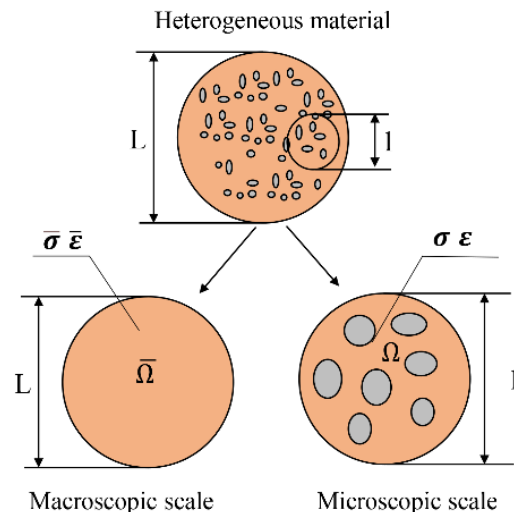


Fig. 1 Illustration of a two scale (macro-micro) problem

Equilibrium equations need to be satisfied on both macroscopic and microscopic scales. The strong form of the macroscopic balance equation reads:

$$\text{Div}(\bar{\sigma}) = 0, \text{ in } \bar{\Omega}, \quad (1a)$$

$$\bar{\sigma} \bar{n} = \bar{t}, \text{ on } \bar{\Gamma}_t, \quad (1b)$$

$$\bar{u} = \bar{u}^*, \text{ on } \bar{\Gamma}_u. \quad (1c)$$

the strong form of the microscopic balance equation reads:

$$\text{Div}(\boldsymbol{\sigma}) = 0, \text{ in } \Omega, \quad (2a)$$

$$\boldsymbol{\varepsilon} = \bar{\boldsymbol{\varepsilon}}, \quad (2b)$$

where: $\bar{\boldsymbol{u}}$ is the macroscopic displacement vector; $\bar{\boldsymbol{n}}$ the unit outward normal vector; $\bar{\Gamma}_t$ the Neumann boundary; $\bar{\boldsymbol{t}}$ the tension on $\bar{\Gamma}_t$; $\bar{\Gamma}_u$ the Dirichlet boundary, respectively.

The macroscopic and microscopic strain and stress fields meet the following volume average theorem [21]:

$$\bar{\boldsymbol{\varepsilon}} = \langle \boldsymbol{\varepsilon} \rangle, \quad (3a)$$

$$\bar{\boldsymbol{\sigma}} = \langle \boldsymbol{\sigma} \rangle. \quad (3b)$$

3. Nonuniform transformation field analysis

The NTFA considers the nonuniform distribution of the microscopic fields. Its key idea is the approximate space-time decomposition of the microscopic plastic strain fields [22]:

$$\boldsymbol{\varepsilon}^p(\boldsymbol{x}, t) \approx \sum_{i=1}^N \xi_i(t) \boldsymbol{\mu}^i(\boldsymbol{x}), \quad (4)$$

where: N represent plastic modes; $\boldsymbol{\mu}^i(\boldsymbol{x})$ are used to approximate the nonuniform distribution of plastic strain field $\boldsymbol{\varepsilon}^p(\boldsymbol{x})$, whereas mode activity coefficients $\xi_i(t)$ are used to characterize the temporal evolution of $\boldsymbol{\varepsilon}^p(\boldsymbol{x}, t)$.

Based on the superposition principle, the microscopic problem Eqs. (2a), (2b) can be decomposed into an elastic problem:

$$\text{Div}(\boldsymbol{C} : \boldsymbol{\varepsilon}_e) = 0, \text{ in } \Omega, \quad (5a)$$

$$\boldsymbol{\varepsilon}_e = \bar{\boldsymbol{\varepsilon}}, \quad (5b)$$

and N eigenstrain problems:

$$\text{Div}(\boldsymbol{C} : (\boldsymbol{\varepsilon}_*^i - \boldsymbol{\mu}^i)) = 0, \text{ in } \Omega, \quad (6a)$$

$$\boldsymbol{\varepsilon}_*^i = 0, \quad i = 1, 2, \dots, N, \quad (6b)$$

where: $\boldsymbol{\varepsilon}_*^i$ represents the total strain tensor.

The solution of elasticity problem Eqs. (5a), (5b) can be written as:

$$\boldsymbol{\varepsilon}(\boldsymbol{x}) = \boldsymbol{A}(\boldsymbol{x}) \bar{\boldsymbol{\varepsilon}}(t), \quad (7a)$$

$$\boldsymbol{\sigma}(\boldsymbol{x}) = \bar{\boldsymbol{C}} \bar{\boldsymbol{\varepsilon}}(t), \quad (7b)$$

where: $\bar{\boldsymbol{C}} = \boldsymbol{C}(\boldsymbol{x}) \boldsymbol{A}(\boldsymbol{x})$ is the equivalent elastic tensor, and

$\boldsymbol{A}(\boldsymbol{x})$ the strain localization operator in micromechanics [23], respectively.

Through superposition of the solutions of elastic problems Eqs. (5a), (5b) and eigen strain problems Eqs. (6a), (6b), the localization criteria of microscopic strains and stresses are obtained as follows:

$$\boldsymbol{\varepsilon}(\boldsymbol{x}) = \boldsymbol{A}(\boldsymbol{x}) \bar{\boldsymbol{\varepsilon}}(t) + \sum_{i=1}^N \xi_i(t) \boldsymbol{\varepsilon}_*^i(\boldsymbol{x}), \quad (8a)$$

$$\boldsymbol{\sigma}(\boldsymbol{x}) = \bar{\boldsymbol{C}} \bar{\boldsymbol{\varepsilon}}(t) + \sum_{i=1}^N \xi_i(t) \boldsymbol{\sigma}_*^i(\boldsymbol{x}). \quad (8b)$$

In Eq. (8b), $\boldsymbol{\sigma}_*^i = \boldsymbol{C}(\boldsymbol{\varepsilon}_*^i - \boldsymbol{\mu}^i)$ is the eigenstress tensor. The macroscopic stress can be obtained by volume averaging of Eq. (8b).

The key problems of the NTFA remain: 1. identification of plastic modes $\boldsymbol{\mu}^i(\boldsymbol{x})$ (Section 4.2 for details); 2. determination of the mode activity coefficient $\xi_i(t)$. Literature [13, 24] mainly showed a phenomenological model (coupled or decoupled) proposed through theoretical derivation. This method requires separate theoretical derivations for each different microscopic constitutive model, so it is not universal and has a high application threshold. The new method to be introduced in Section 4 will solve this problem well.

4. Cluster-based nonuniform transformation field analysis (CNTFA) and numerical implementation

4.1. Clustering of the RVE

Clustering analysis is carried out for representative volume element (RVE), and all units are divided into I clusters. Eq. (4) is simplified as:

$$\boldsymbol{\varepsilon}^{p,I}(\boldsymbol{x}, t) \approx \sum_{i=1}^M \xi_i(t) \boldsymbol{\mu}_i^I, \quad (9)$$

the Eqs. (8a) and (8b) become:

$$\boldsymbol{\varepsilon}^I = \boldsymbol{A}^I \bar{\boldsymbol{\varepsilon}}(t) + \sum_{i=1}^M \xi_i(t) \boldsymbol{\varepsilon}_{i*}^I, \quad (10a)$$

$$\boldsymbol{\sigma}^I = \boldsymbol{C}^I \boldsymbol{A}^I \bar{\boldsymbol{\varepsilon}}(t) + \sum_{i=1}^M \xi_i(t) \boldsymbol{\sigma}_{i*}^I. \quad (10b)$$

Each cluster is composed of a single material phase, where its internal stress and strain fields are approximately considered to be uniform. The relationship between the stress and strain of each cluster follows the local constitutive relationship of its material phase, as suggested in [25].

4.2. Mode identification

The plastic mode $\boldsymbol{\mu}_i^I$ should fully represent the nonuniform distribution of the plastic strain field of composite materials, whereas its number should be as small as possible, so as to achieve the purpose of effective order reduction. Firstly, under different strain paths (such as tension and shear), the finite element pre-analysis of the RVE is carried out. Then, the average plastic strain within each cluster is calculated, thus obtaining N_s typical snapshots of the plastic

strain field $\boldsymbol{\varepsilon}_i^{p,l}$. Those snapshots are decomposed by the Karhunen–Loève algorithm to calculate the eigenvalues of the correlation matrix λ_l and eigenvector \boldsymbol{g}_l . There holds the cut-off criterion:

$$\beta \left(\sum_{l=1}^{N_s} \lambda_l \right) \leq \left(\sum_{k=1}^M \lambda_k \right), \quad (11)$$

where: the constant $0 \leq \beta \leq 1$ represents the proportion of information contained in M eigenvectors among N_s eigenvectors [19]. In this paper, we choose $\beta = 0.999$.

Finally, the plastic mode $\boldsymbol{\mu}_i^l$ can be obtained by using the computed eigenvector \boldsymbol{g}_k and plastic strain field snapshot $\boldsymbol{\varepsilon}_i^{p,l}$. Formally we have:

$$\boldsymbol{\mu}_i^l = \sum_{l=1}^{N_s} \boldsymbol{g}_l^l \boldsymbol{\varepsilon}_i^{p,l}, \quad i \in [1, M]. \quad (12)$$

4.3. Online computation

The main task of the online computation is to calculate the mode activity coefficient ξ_i at the current time step ($k+1$). For a given macroscopic strain $\bar{\boldsymbol{\varepsilon}}_{k+1}$, we first initialize the mode activity coefficient increment as $(\Delta \xi_i)_{k+1}^0 = 0$, where j represents iterative steps. The iteration

$$(\Delta \xi_i)_{k+1}^j = \underset{\Delta \xi_i}{\operatorname{argmin}} \frac{\sum_I w_I \left\| (\Delta \boldsymbol{\varepsilon}^{p,l})_{k+1}^j - \sum_{i=1}^N \Delta \xi_i \boldsymbol{\mu}_i^l \right\|^2}{\sum_I \left\| (\Delta \boldsymbol{\varepsilon}^{p,l})_{k+1}^j \right\|^2}. \quad (16)$$

The analytical solution of the above problem is as follows:

$$(\Delta \xi_i)_{k+1}^j = \left(\sum_I w_I \left(\sum_{i=1}^M \boldsymbol{\mu}_i^l : \boldsymbol{\mu}_i^l \right) \right)^{-1} \left(\sum_I w_I \left((\Delta \boldsymbol{\varepsilon}^{p,l})_{k+1}^j : \boldsymbol{\mu}_i^l \right) \right). \quad (17)$$

When the termination condition Eq. (13) is satisfied, the iteration is terminated. The mode activity coefficients, plastic strain and macro stress are updated as follows:

$$(\xi_i)_{k+1} = (\xi_i)_k + (\Delta \xi_i)_{k+1}^j, \quad (18a)$$

$$(\boldsymbol{\varepsilon}^{p,l})_{k+1} = (\boldsymbol{\varepsilon}^{p,l})_k + \sum_{i=1}^M (\Delta \xi_i)_{k+1} \boldsymbol{\mu}_i^l, \quad (18b)$$

$$(\bar{\boldsymbol{\sigma}})_{k+1} = \frac{1}{V} \sum_I V^I (\boldsymbol{\sigma}^I)_{k+1}, \quad (18c)$$

where: $(\boldsymbol{\varepsilon}^{p,l})_k$ and V^I are the plastic strain of the last time step k and the volume of the cluster I , respectively.

4.4. Numerical implementation

The overall numerical implementation framework is shown in Fig.2.

termination condition is $res < tol$. The residual res is defined as:

$$res = \frac{\sum_i \left[(\Delta \xi_i)_{k+1}^j - (\Delta \xi_i)_{k+1}^{j-1} \right]^2}{\sum_i \left[(\Delta \xi_i)_{k+1}^j \right]^2}, \quad (13)$$

while tol is the tolerance.

After time discretization, Eq. (10a) becomes:

$$(\boldsymbol{\varepsilon}^I)_{k+1}^j = \mathbf{A}^I : (\bar{\boldsymbol{\varepsilon}}_{k+1}) + \sum_{i=1}^M \left((\xi_i)_k + (\Delta \xi_i)_{k+1}^{j-1} \right) \boldsymbol{\varepsilon}_{i^*}^I, \quad (14)$$

where: $(\xi_i)_k$ is the mode activity coefficient of the last time step. According to the local constitutive relation, the plastic strain increment $(\Delta \boldsymbol{\varepsilon}^{p,l})_{k+1}^j$ can be obtained from Eq. (13). According to Eq. (9), the plastic strain increment can also be expressed as:

$$(\Delta \boldsymbol{\varepsilon}^{p,l})_{k+1}^j \approx \sum_{i=1}^M (\Delta \xi_i)_{k+1}^j \boldsymbol{\mu}_i^l. \quad (15)$$

As suggested in [19], the mode activity coefficient increment $(\Delta \xi_i)_{k+1}^j$ can be determined by solving the following least squares optimization problem:

For the RVE modeling, we consider randomly distributed graphene nanosheets (GNSs) in a graphene nanocomposite. As shown in Fig. 3, we use ANSYS Parametric Design Language to write programs to automatically generate three-dimensional RVE models. The generated RVE model is then analysed in our self-programmed MATLAB codes. For simplicity, each GNS is modeled as a circular disk with a diameter of 200 nm and a thickness of 10 nm, while the RVE is considered as a cube with a side-length of 1000 nm.

For the graphene nanocomposites (the RVE model as shown in Fig. 4 and Fig. 7), the following nonlinear hardening equation is used to characterize the isotropic hardening of the matrix:

$$R(q) = Hq + c(1 - \exp(-bq)), \quad (19)$$

where: H , c and b are material parameters and q is the equivalent plastic strain.

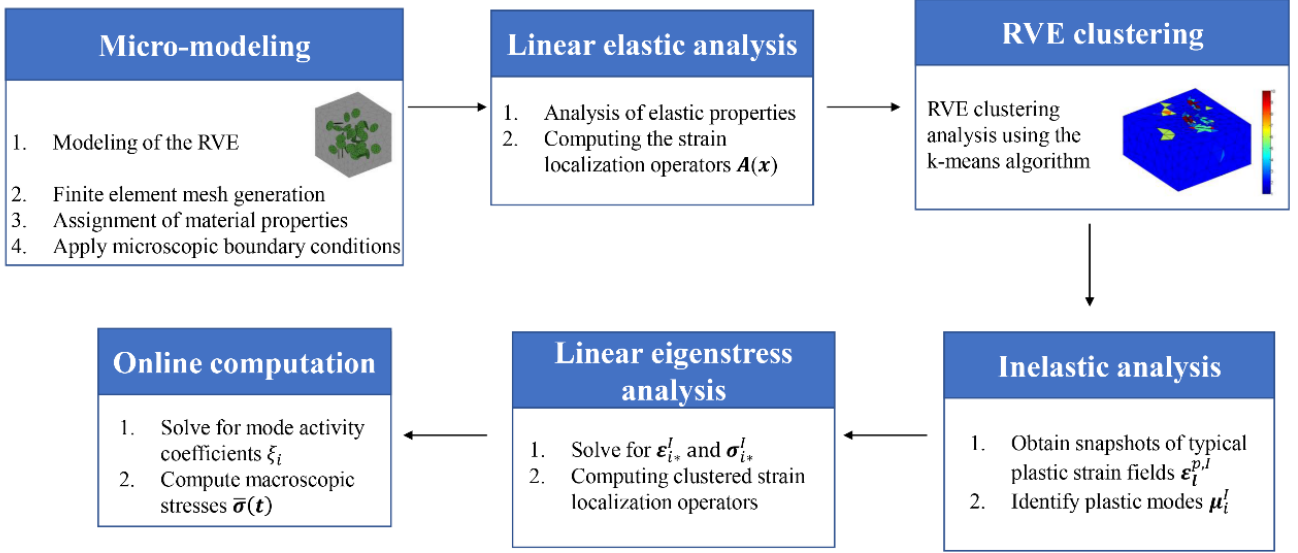


Fig. 2 Flowchart of cluster non-uniform transformation field analysis for graphene nanocomposites

In this paper, linear displacement boundary conditions are used. Apply displacement constraints to all nodes on the RVE boundary through MATLAB programming. And the subsequent analysis is completed in MATLAB.

$$\underline{u}_n = [u_1 \quad u_2 \quad u_3]_n^T, \quad (20a)$$

$$\underline{X}_n = \frac{1}{2} \begin{bmatrix} 2x_1 & 0 & 0 \\ 0 & 2x_2 & 0 \\ 0 & 0 & 2x_3 \\ x_2 & x_2 & 0 \\ 0 & x_2 & x_2 \\ x_2 & 0 & x_2 \end{bmatrix}_n^T, \quad (20b)$$

$$\underline{\bar{\varepsilon}} = [\bar{\varepsilon}_{11} \quad \bar{\varepsilon}_{22} \quad \bar{\varepsilon}_{33} \quad 2\bar{\varepsilon}_{12} \quad 2\bar{\varepsilon}_{23} \quad 2\bar{\varepsilon}_{13}]^T \quad (20c)$$

In order to calculate the strain localization operator, six orthogonal bases [26] are introduced:

$$\begin{aligned} \Sigma^1 &= \mathbf{e}_i \otimes \mathbf{e}_i, \quad i = 1, 2, 3 \\ \Sigma^4 &= \text{sym}(\mathbf{e}_1 \otimes \mathbf{e}_2) \\ \Sigma^5 &= \text{sym}(\mathbf{e}_1 \otimes \mathbf{e}_3) \\ \Sigma^6 &= \text{sym}(\mathbf{e}_2 \otimes \mathbf{e}_3) \end{aligned} \quad (21)$$

For three-dimensional problems. Next, we solve 6 linear elastic problems:

$$\text{Div}(\sigma_e^i) = \text{Div}(\mathbf{C}\varepsilon_e^i) = 0, \quad \text{in } \Omega, \quad (22a)$$

$$\varepsilon_e^i = \varepsilon_0 \Sigma^i, \quad \text{for } i = 1, \dots, 6, \quad (22b)$$

where: ε_0 is a constant. The strain localization operator $\mathbf{A}(\mathbf{x})$ is:

$$\mathbf{A}(\mathbf{x}) = \frac{1}{\varepsilon_0} \sum_{i=1}^{N_d=6} \varepsilon_e^i(\mathbf{x}) \otimes \Sigma^i. \quad (23)$$

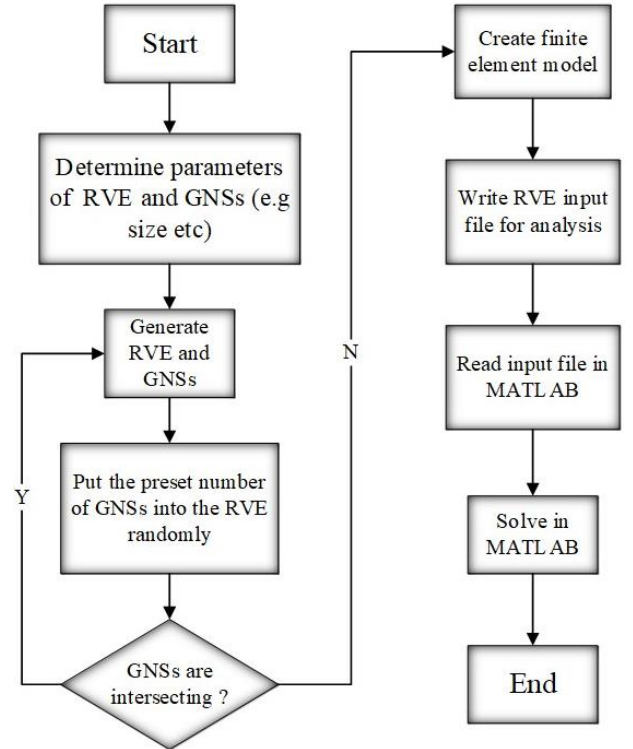


Fig. 3 Flowchart of RVE modeling for graphene nanocomposites

For each cluster, \mathbf{A}^l can be obtained by volume averaging of $\mathbf{A}(\mathbf{x})$ in Eq. (23).

The microscopic elastic strain field is completely determined by $\mathbf{A}(\mathbf{x})$. Hence, it can be used as an important index to investigate the distribution characteristics of the microscopic elastic strain fields. This paper uses k-means clustering algorithm to subdivide the RVE into different clusters, based on \mathbf{A} values of different finite elements. Each cluster does not interfere with each other, and each cluster consists of a single material phase. As shown in Fig. 5, the RVE is divided into 10 clusters using the above algorithm for illustration.

Provided those plastic modes μ_i^l are obtained through mode identification in Section 4.2, N linear eigenstress problems are solved:

$$\text{Div}\left(\mathbf{C} : (\boldsymbol{\varepsilon}_{i*}^l - \boldsymbol{\mu}_i^l)\right) = 0, \text{ in } \Omega, \quad (24a)$$

$$\boldsymbol{\varepsilon}_{i*}^l = 0, \quad i = 1, 2, \dots, N, \quad (24b)$$

$$\boldsymbol{\sigma}_{i*}^l = \mathbf{C} (\boldsymbol{\varepsilon}_{i*}^l - \boldsymbol{\mu}_i^l), \quad (24c)$$

the eigen strain field $\boldsymbol{\varepsilon}_*^{i,l}$ required by Eq. (14) is calculated.

Finally, the mode activity coefficient ξ_i and the macro stress $\bar{\boldsymbol{\sigma}}$ at the current time step are determined through online analysis in Section 4. 3.

5 Numerical examples

5.1. Validation of the cluster-based nonuniform transformation field analysis

Graphene nanocomposites are studied here. As shown in Fig. 4, the graphene nanosheets are distributed in an undirected manner, accounting for 1% of the total volume. Graphene is assumed to be linear elastic. The epoxy resin matrix is considered as an elastoplastic material, where the classical von Mises plasticity model is used. We use the material parameters given in Table 1 obtained from a calibration with the experimental data in [27]. As shown in Fig. 5, the RVE model is divided into 10 clusters by k-means clustering algorithm. Five different plastic modes were identified by the Karhunen-Loève decomposition. For illustration, Table 2 shows two of them.

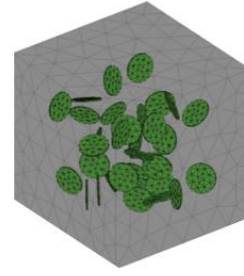


Fig. 4 RVE of graphene nanocomposite

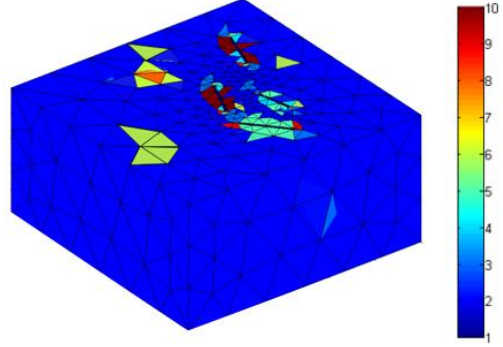


Fig. 5 RVE clustering of graphene nanocomposites returned by the k-means algorithm

Table 1

Material properties of graphene nanocomposite

Material	Young's modulus, GPa	Poisson ratio	Yield stress, MPa	H , MPa	B , -	C , MPa
Matrix	3	0.3	50	40	10	200
GNSs	1050	0.186	-	-	-	-

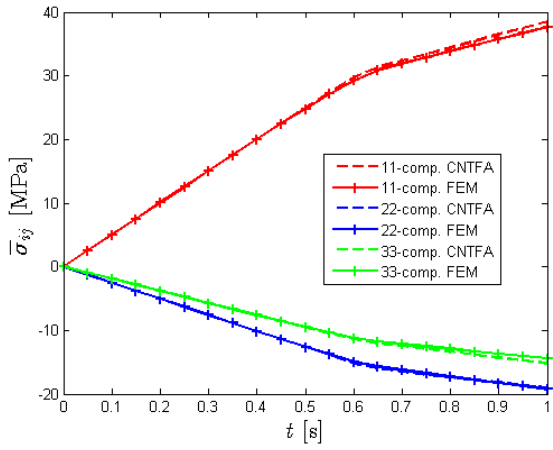
Table 2

Two plastic modes identified by the Karhunen-Loève decomposition

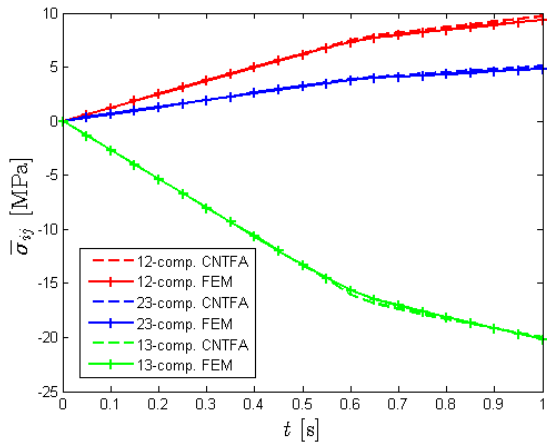
	I	1	2	3	4	5	6	7	8	9	10
μ_1^l	$\mu_{1,11}^l$	0	-0.7597	-0.0695	-1.0957	-0.7090	-3.1487	-0.8504	-1.2599	-1.1818	-0.5450
	$\mu_{1,22}^l$	0	0.4358	0.0573	0.2316	0.4700	1.6113	0.4097	1.0115	0.6530	0.3016
	$\mu_{1,33}^l$	0	0.3239	0.0122	0.8641	0.2390	1.5374	0.4406	0.2485	0.5289	0.2435
	$\mu_{1,12}^l$	0	0.0028	0.0177	-0.0187	-0.0652	0.0006	0.0052	0.0116	0.1027	0.0492
	$\mu_{1,23}^l$	0	0.0105	-0.0069	-0.0093	0.0017	0.0428	-0.0100	-0.0395	0.2226	-0.0054
	$\mu_{1,13}^l$	0	0.0059	0.0016	0.0084	-0.0157	0.0237	0.0000	-0.0045	-0.0057	-0.0070
μ_2^l	I	1	2	3	4	5	6	7	8	9	10
	$\mu_{2,11}^l$	0	-0.4955	-0.0548	0.6880	-0.0871	5.2688	-0.5369	0.7878	0.6443	-0.1322
	$\mu_{2,22}^l$	0	0.2866	0.0470	-0.0954	0.0567	-2.6888	0.2657	-0.5993	-0.3686	0.0695
	$\mu_{2,33}^l$	0	0.2089	0.0078	-0.5926	0.0304	-2.5801	0.2712	-0.1886	-0.2757	0.0627
	$\mu_{2,12}^l$	0	0.0083	0.0069	0.0053	0.0676	-0.0067	0.0019	0.0065	-0.2031	-0.1220
	$\mu_{2,23}^l$	0	0.0106	-0.0083	0.0182	-0.0112	-0.0747	-0.0003	0.0213	-0.1151	0.0333
	$\mu_{2,13}^l$	0	0.0059	-0.0006	-0.0321	0.0032	-0.0707	-0.0008	0.0280	-0.0451	0.0389

Fig. 6 gives a comparison of the macroscopic stresses and the macroscopic strain power between the CNTFA and the FEM. The macro stress components computed by both methods are completely identical in the elastic stage. Compared with the finite element computation, the

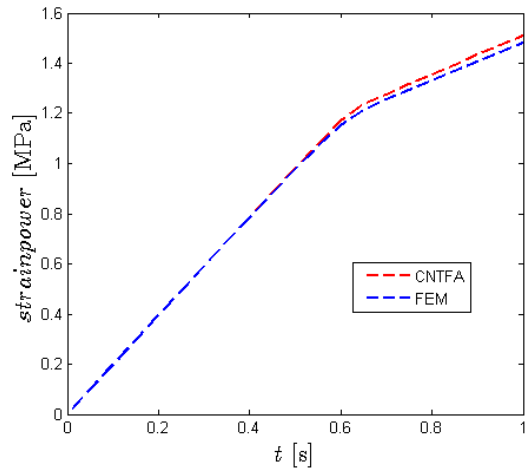
CNTFA results show slight deviation in the plastic stage, whereas the acceleration rate is up to 4500.



a



b



c

Fig. 6 Comparison of the macroscopic prediction between the CNTFA and the FEM: a) Macroscopic stresses - Part I; b) Macroscopic stresses - Part II; c) Strain power

5.1. Uniaxial tensile simulation of graphene nanocomposites

In this Section, the CNTFA method is used to study the uniaxial tensile response of the composites with different graphene volume fraction. Figs. 4, 7, a and b show the RVE models with a graphene volume fraction of 1%, 1.5% and 0.5%, respectively. The material parameters are the same as those in Table 1.

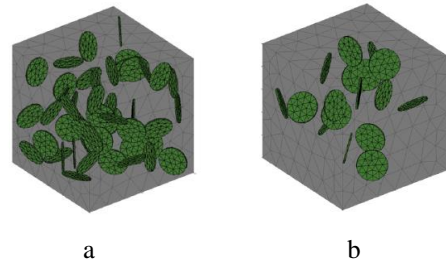


Fig. 7 RVE model of graphene nanocomposites with different graphene contents: a) 1.5%; b) 0.5%

To validate our models, we use the experimental data in [27] for reference. As shown in Fig. 8, for a graphene volume fraction of 0.5%, compared to the experimental data of a uniaxial test in [27], both the CNTFA and the FEM render quite accurate predictions.

In the following, we use CNTFA models to predict the uniaxial tensile responses of graphene nanocomposites with different contents of GNSs. Fig. 9 shows the comparative results of strain-stress curves of the composites with different GNSs volume fractions in different directions. In the elastic and plastic stages, the strength of the material increases with increasing GNSs content.

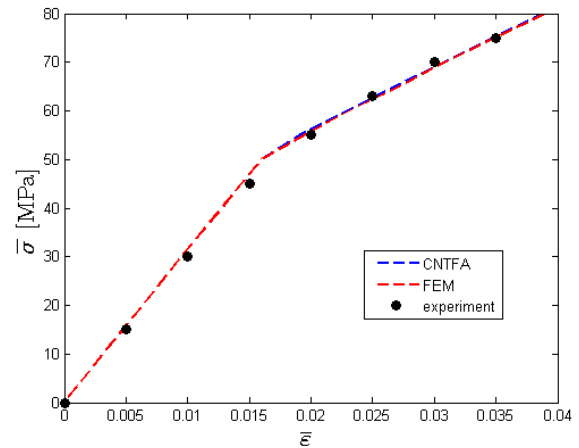
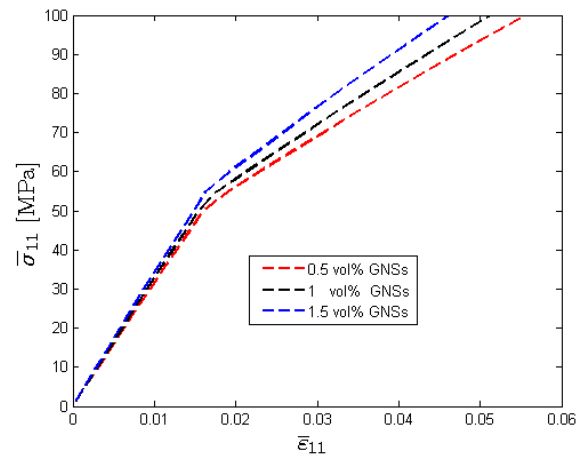
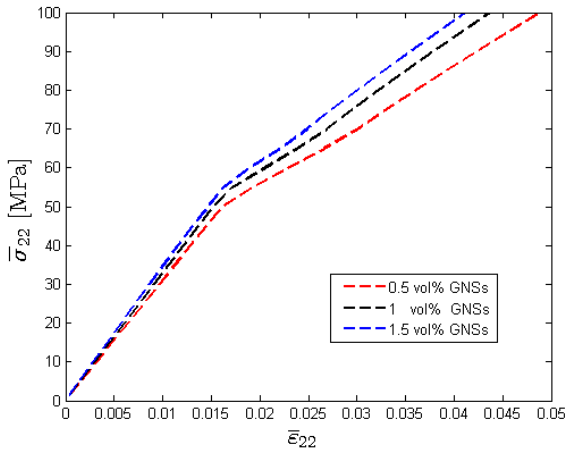


Fig. 8 Comparison of uniaxial stress-strain curves between CNTFA/FEM predictions and experimental data in [27]

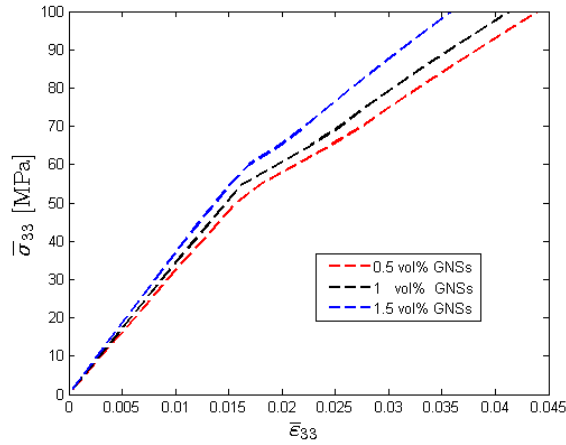


a

Fig. 9 Macroscopic stress-strain curves of graphene nanocomposites with different GNSs volume fractions: a) Macroscopic stresses - Part I; b) Macroscopic stresses - Part II; c) Macroscopic stresses - Part III



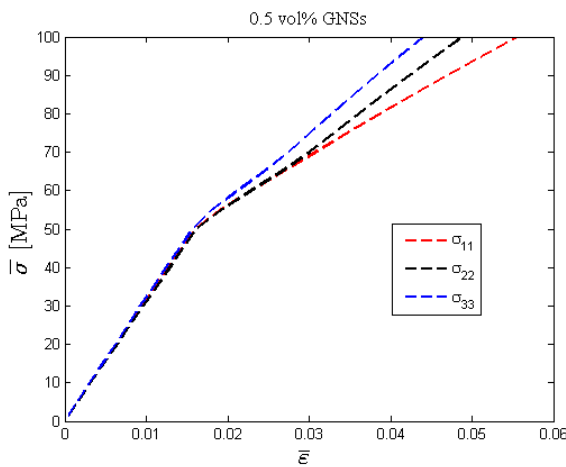
b



c

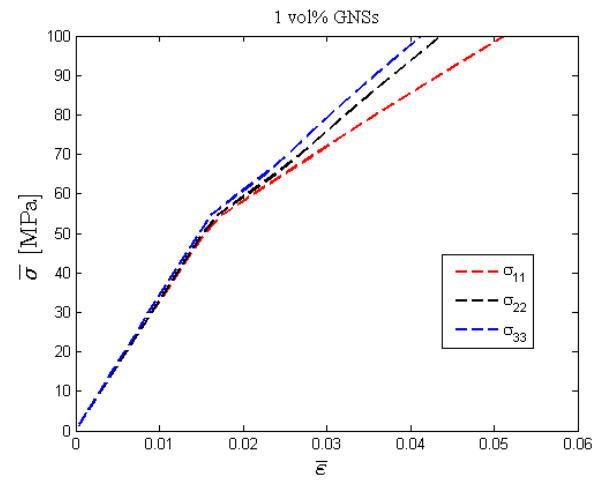
Fig. 9 Continuation

Fig. 10 shows the comparison of uniaxial tensile stress-strain curves in different directions with fixed graphene content. The curves in three different directions are very close in the elastic stage, and there is obvious deviation in the plastic stage. This indicates the anisotropy of the considered graphene nanocomposite. Although a random distribution of GNSs is considered, the limited number of GNSs in the RVE is not sufficient to recover an isotropic response.

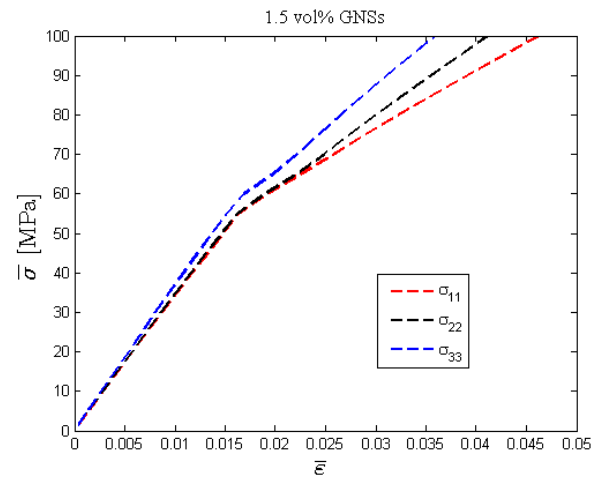


a

Fig. 10 Macroscopic stress-strain curves of graphene nanocomposites with different graphene volume fractions in different directions: a) Part I; b) Part II; c) Part III



b



c

Fig. 10 Continuation

6. Conclusion

1. Combining the nonuniform transformation field analysis method with the k-means clustering algorithm, an improved reduced order model is proposed as suggested in [19]. The model improves on the defects of the original NTFA method, such as low universality and high application threshold. Users can easily embed any microscopic constitutive model into the reduced order framework of this paper according to their own needs without having to derive the reduced order model separately.

2. The CNTFA method can efficiently and reasonably predict the macroscopic mechanical response of composites. Compared with the traditional finite element computation, an acceleration rate of 10^3 - 10^4 has been reached.

3. The influence of the evolution of the material mesoplastic field on the macro response is revealed using the CNTFA method. For simplicity, this paper only compares and analyzes the composite materials with different graphene contents, which shows the effectiveness of this method. The method in this paper will be extended to the research of optimal material design and performance prediction of novel nanocomposites.

Acknowledgments

The work described in this paper was supported by the National Natural Science Foundation of China (Grant Nos. 12002309, 51875523, 52275164), the Zhejiang Provincial Natural Science Foundation of China (Grant No: LQ21A020002).

References

1. **Wang, J.; Qian, L.; Yuang, R.** 2007. Thermal residual stresses in composite material barrel, *Journal of Ballistics* 19(1): 82-85.
<https://doi.org/10.1002/jrs.1570>.
2. **Lee, C.; Wei, X.; Kysar, J. W.; Hone, J.** 2008. Measurement of the elastic properties and intrinsic strength of monolayer graphene, *Science* 321(5887): 385-388.
<https://doi.org/10.1126/science.1157996>.
3. **Rafiee, M. A.; Rafiee, J.; Wang, Z.; et al.** 2009. Enhanced mechanical properties of nanocomposites at low graphene content, *ACS Nano* 3(12): 3884-3890.
<https://doi.org/10.1021/nm9010472>.
4. **Huang, X.; Qi, X.; Boey, F.** et al. 2012. Graphene-based composites, *Chemical Society Reviews* 41(2): 666-686.
<https://doi.org/10.1039/c1cs15078b>.
5. **Ohno, N.; Narita, K.; Okumura, D.** 2018. Homogenized elasticviscoplastic behavior of plate-fin structures with two pore pressures, *International Journal of Impact Engineering* 86: 18-25.
<https://doi.org/10.1016/j.ijmecsci.2013.10.015>.
6. **Geers, M.; Kouznetsova, V.; Matouš, K.** 2017. Homogenization methods and multiscale modeling: nonlinear problems, *Encyclopedia of Computational Mechanics Second Edition*, p. 1-34.
<https://doi.org/10.1002/9781119176817.ecm2107>.
7. **Fritzen, F.; Leuschner, M.** 2013. Reduced basis hybrid computational homogenization based on a mixed incremental formulation, *Computer Methods in Applied Mechanics and Engineering* 260: 143-154.
<https://doi.org/10.1016/j.cma.2013.03.007>.
8. **Fritzen, F.; Hodapp, M.** 2016. The finite element square reduced (FE2R) method with GPU acceleration: towards three-dimensional two-scale simulations, *International Journal for Numerical Methods in Engineering* 107: 853-881.
<https://doi.org/10.1002/nme.5188>.
9. **Ri, J. H.; Hong, H. S.** 2019. A basis reduction method using proper orthogonal decomposition for lower bound shakedown analysis of kinematic hardening material, *Computational Mechanics* 64: 1-13.
<https://doi.org/10.1007/s00466-018-1653-y>.
10. **Dvorak, G. J.; Bahei-El-Din, Y. A.; Wafa, A. M.** 1994. Implementation of the transformation field analysis for inelastic composite materials, *Computational Mechanics* 14(3): 201-228.
<https://doi.org/10.1007/BF00370073>.
11. **Prochazka, P.** 1999. Homogenization of nonlinear composites using transformation field analysis, *Journal of the Chinese Institute of Engineers* 22(6): 721-727.
<https://doi.org/10.1080/02533839.1999.9670508>.
12. **Fish, J.; Filonova, V.; Yuan, Z.** 2013. Hybrid incompatible eigenstrain based homogenization, *International Journal for Numerical Methods in Engineering* 95(1): 1-32.
<https://doi.org/10.1002/nme.4473>.
13. **Largent, R.; Michel, J. C.; Suquet, P.** 2014. Extension of the nonuniform transformation field analysis to linear viscoelastic composites in the presence of aging and swelling, *Mechanics of Materials* 74: 76-100.
<https://doi.org/10.1016/j.mechmat.2014.02.004>.
14. **Ju, X.; Mahnken, R.** 2016. An NTFA-based homogenization framework considering softening effects, *Mechanics of Materials* 96: 106-125.
<https://doi.org/10.1016/j.mechmat.2016.01.007>.
15. **Ju, X.; Mahnken, R.** 2021. A nonuniform transformation field analysis for composites with strength difference effects in elastoplasticity, *International Journal of Solids and Structures* 228: 111103.
<https://doi.org/10.1016/j.ijsolstr.2021.111103>.
16. **Liu, Z.; Bessa, M.; Liu, W. K.** 2016. Self-consistent clustering analysis: an efficient multiscale scheme for inelastic heterogeneous materials, *Computer Methods in Applied Mechanics and Engineering* 306: 319-341.
<https://doi.org/10.1016/j.cma.2016.04.004>.
17. **Liu, Z.; Fleming, M.; Liu, W. K.** 2018. Microstructural material database for self-consistent clustering analysis of elastoplastic strain softening materials, *Computer Methods in Applied Mechanics and Engineering* 330: 547-577.
<https://doi.org/10.1016/j.cma.2017.11.005>.
18. **Han, X.; Xu, C.; Xie, W.; Meng, S.** 2019. Multiscale computational homogenization of woven composites from microscale to mesoscale using data-driven self-consistent clustering analysis, *Composite Structures* 220: 760-780.
<https://doi.org/10.1016/j.compstruct.2019.03.053>.
19. **Jun-Hyok Ri; Un-Il Ri; Hyon-Sik Hong.** 2021. Multiscale analysis of elastic-viscoplastic composite using a cluster-based reduced order model, *Composite Structures* 272: 114209.
<https://doi.org/10.1016/j.compstruct.2021.114209>.
20. **Kanouté, P.; Boso, D. P.; Chaboche, J. L.; Schrefler, B.A.** 2009. Multiscale methods for composites: a review, *Archives of Computational Methods in Engineering* 16(1): 31-75.
<https://doi.org/10.1007/s11831-008-9028-8>.
21. **Hill, R.** 1963. Elastic properties of reinforced solids: some theoretical principles, *Journal of the mechanics and physics of solids* 11: 357-372.
[https://doi.org/10.1016/0022-5096\(63\)90036-X](https://doi.org/10.1016/0022-5096(63)90036-X).
22. **Roussette, S.; Michel, J. C.; Suquet, P.** 2009. Nonuniform transformation field analysis of elastic-viscoplastic composites, *Composites Science and Technology* 69: 22-27.
<https://doi.org/10.1016/j.compscitech.2007.10.032>.
23. **Gusev, A. A.** 2017. Finite element estimates of viscoelastic stiffness of short glass fiber reinforced composites, *Composite Structures* 171: 53-62.
<https://doi.org/10.1016/j.compstruct.2017.03.021>.
24. **Cheng, G. D.; Li, X. K.; Nie, Y. H.; Li, H. Y.** 2019. FEM-cluster based reduction method for efficient numerical prediction of effective properties of heterogeneous material in nonlinear range, *Computer Methods in Applied Mechanics and Engineering* 348: 157-184.
<https://doi.org/10.1016/j.cma.2019.01.019>.

25. **Nie, Y. H.; Cheng, G. D.; Li, X. K.; Xu, L. A.; Li, K.** 2019. Principle of cluster minimum complementary energy of FEM-cluster-based reduced order method: fast updating the interaction matrix and predicting effective nonlinear properties of heterogeneous material, *Computational Mechanics* 64(2): 323–349. <https://doi.org/10.1007/s00466-019-01710-6>.
26. **Fritzen, F.; Böhlke, T.** 2010. Three-dimensional finite element implementation of the nonuniform transformation field analysis, *International Journal for Numerical Methods in Engineering* 84(7): 803–829. <https://doi.org/10.1002/nme.2920>.
27. **Lee, M. W.; Wang, T. Y.** 2016. Mechanical properties of nanocomposites with functionalized graphene, *Journal of Composite Materials* 50(27): 3779–3789. <https://doi.org/10.1177/0021998315625788>.

Y. Jiang, J. Chen, L. Liang, Y. Xu, X. Ju

CLUSTER-BASED NONUNIFORM TRANSFORMATION FIELD ANALYSIS OF GRAPHENE NANOCOMPOSITES

S u m m a r y

Graphene nanocomposites have attracted much attention in materials science due to their superior mechanical

properties. It is difficult for conventional multiscale methods to provide substantial assistance to the research of such materials due to their huge computational costs. Nonuniform transformation field analysis is a very effective reduced order homogenization method for elastoplastic multiscale analysis. However, the reduced order model derived from this method has the shortcoming of low universality and high application threshold. As suggested in [19], an improved reduced order model is proposed by combining the nonuniform transformation field analysis with the k-means clustering algorithm. One can embed the required microscopic constitutive model into the reduced order homogenization framework without the need to derive a new reduced order model. Based on the cluster-based nonuniform transformation field analysis, the influence of the microscopic plastic strain field evolution on the macroscopic response of the material under consideration is revealed, while the mechanical properties of graphene nanocomposites are predicted. The numerical results show that the new reduced order model can accurately predict the macroscopic mechanical properties of composite materials, and its acceleration rate compared to the traditional finite element computations reaches 10^3 - 10^4 .

Keywords: graphene, nanocomposites, reduced order model, multiscale methods, clustering, nonuniform, transformation field analysis.

Received January 12, 2023

Accepted August 2, 2023



This article is an Open Access article distributed under the terms and conditions of the Creative Commons Attribution 4.0 (CC BY 4.0) License (<http://creativecommons.org/licenses/by/4.0/>).